Turkish Journal of Electrical Engineering & Computer Sciences

http://journals.tubitak.gov.tr/elektrik/

Research Article

Turk J Elec Eng & Comp Sci
(2016) 24: 3792 – 3806

doi:10.3906/elk-1502-198

Adaptive speed observer with disturbance torque compensation for sensorless induction motor drives using RT-Lab

Mohan KRISHNA*, Febin DAYA
School of Electrical Engineering, VIT University, Chennai Campus, Chennai, Tamil Nadu, India

Received: 23.02.2015 • **Accepted/Published Online:** 11.06.2015 • **Final Version:** 20.06.2016

Abstract: This paper presents an improved version of the extended Luenberger observer with joint estimation of rotor speed and disturbance torque. The mechanical model of the induction motor is also utilized for the estimation of disturbance torque to add to the robustness of the observer. The estimated disturbance torque is treated as a model disturbance and physically incorporated into the observer state dynamic equation. The dynamic performance and efficacy of the modified observer is tested for variations in external load and inertia coefficient in the mechanical model. The above observer model is first built offline, using MATLAB/Simulink block sets, and simulated. Further, the offline simulated results are validated in real time by incorporating RT-Lab block sets into the Simulink model and implementing it in the OP4500 real-time simulator developed by Opal-RT. The implementation of the above concept in a relatively new real-time environment adds more strength to the offline findings and provides an exact replica of how the actual physical system would behave.

Key words: Disturbance torque, extended Luenberger observer, induction motor, model reference adaptive systems, Opal-RT, speed estimation

1. Introduction

The significance of estimating the speed of an induction motor is to do away with additional electronics, cost, and mounting space that can otherwise be attributed to the use of a speed encoder. Either the magnetic saliencies of the rotor or the machine model can be exploited to estimate the speed. Though the former is a more accurate means of speed measurement, it introduces considerable measurement delay and hence cannot be used for feedback. However, in case of the machine model-based speed estimation scheme, the ease of implementation is compromised by the sensitivity to parameter variations. Adaptive speed estimation techniques fed from the terminal quantities of the machine are employed for speed sensorless induction motor drives for the purpose of parameter estimation. The extended model reference adaptive system (MRAS) speed observer or the Luenberger observer method is a popular parameter estimation technique, as it is easily implementable and adapts itself quickly to the controlled system [1–9]. Several configurations of the above scheme are used for estimating a single unknown parameter or simultaneous and sequential estimation of two or more unknown parameters. There were also comparative studies of several inherently adaptive speed observers in terms of speed tracking and online identification of parameters [10,11]. The adaptive and sliding mode approaches were evaluated for parameter sensitivity in a real-time laboratory setup using a peripheral component interface card and PCLD-8710 I/O terminal with a measurement interface. The sliding mode approach showed better performance for variations in

*Correspondence: smk87.genx@gmail.com

rotor resistance and stator resistance. Illas et al. [12] investigated several sensorless speed estimation schemes involving rotor slotting, Kalman filters, and MRAS-based estimators and observers. There is instability and degradation in the performance of the observers at operating speeds of less than 25 rpm due to mismatch in values of certain parameters, like the stator resistance and rotor time constant. The experimental verification of the MRAS-based speed observer approaching very low and zero speed ranges was performed in [13] by means of a dSPACE-based control platform. There are also several methods involving simultaneous estimation of parameters by mutual MRAS estimators, in which the roles of the reference and the adaptive models are interchanged depending on the parameter to be adapted, one of which was proposed by [14]. There are also observer schemes for estimating various types of disturbances primarily used in negating the effect of the load torque on the speed. Mihai et al. [15] implemented two disturbance torque observers, one using the mechanical model and the other based on a reduced-order Gopinath method in order to reject the effect of the load torque on the estimation of speed. Several schemes focused on simultaneous estimation of the disturbance torque or load torque along with the rotor speed and other parameters like stator resistance; observers were also modeled with exact disturbances [16–19].

So far, existing research on the above concept was validated on several experimental platforms without disturbance torque compensation. Though some schemes did have disturbances modeled in their structure, whose gains depended on the stator frequency, they were not validated in real time. The objective of this research is to present an improved and more robust observer by incorporating the estimated disturbance torque into the observer state dynamic equation as a model disturbance. To increase efficacy, disturbance torque is estimated by exploiting the mechanical model of the induction motor and the dynamic performance of the joint state observer is analyzed for changes in the external load torque and inertia coefficient of the mechanical model. The findings of the improved mechanism are further validated in an RT-Lab-based real-time platform using an OP4500 simulator. Closer analysis of the results provide more clarity regarding the observer performance in real time as compared to offline. The basic theories behind MRAS and other adaptive parameter estimation schemes are presented in Section 2. It is followed by the dynamic model of the induction motor and the structure of the observer with disturbance torque estimation and compensation in Section 3. An insight into the concept of real-time simulation and the RT-Lab-based distributed real-time simulation platform is given in Section 4. Next, the offline and real-time simulated results are presented in Section 5 for different test cases, followed by an elaborate discussion in Section 6 and the conclusion in Section 7. The parameters and ratings of the motor used for the study are given in the Appendix.

2. MRAS and adaptive speed estimation schemes

Any adaptive system, in addition to a feedback mechanism, compensates for variations in operating conditions, process dynamics, and disturbances, thereby providing an optimal performance. The popularly used adaptive parameter estimation schemes fed from the machine model are shown in Figure 1. In this paper, the influence of the estimated speed and the estimated disturbance torque on the behavior of the observer system is an adaptive feature. The simplest configuration is the MRAS shown in Figure 2. The principle of the MRAS strategy can be explained by means of a mathematical model, the reference model, which denotes the desired performance of the system, and the adjustable model (or the adaptive model) [20]. When there is a deviation in the performance of the adaptive model from the ideal behavior of the reference model, either the controller parameters are adjusted or an additional input is added to the process dynamics. This gives rise to an optimization problem, i.e. minimization of the error vector between the reference and the adaptive models or convergence of the error vector to zero.

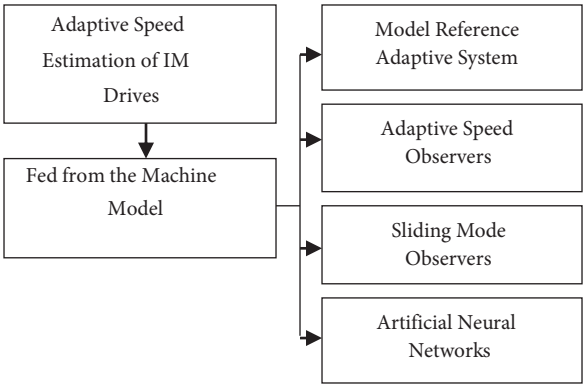

Figure 1. Classification of speed estimation methods.

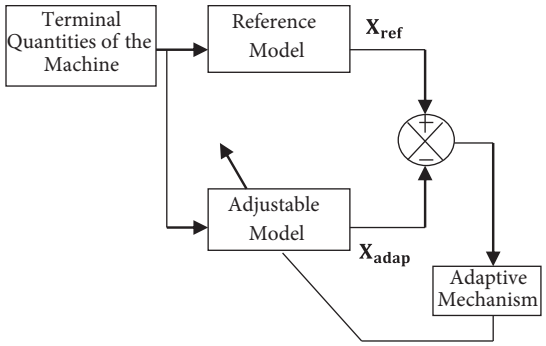

Figure 2. General configuration of parameter adaptive MRAS.

$$Z = \int_0^T e^2 dt, \tag{1}$$

where Z is the optimization criterion, and

$$e = X_{ref} - X_{adap}, \tag{2}$$

where e is the error vector and X_{ref} and X_{adap} are the reference model and adaptive model outputs, respectively. The quantity that is selected as the output of the reference and adjustable models determines the type of the MRAS configuration. Some of the popular choices are rotor flux, back-EMF, stator currents, and instantaneous reactive power. The extended MRAS observer used in this paper involves a higher-order and more accurate model, which is more robust regarding parameter sensitivity and disturbance rejection.

3. Induction motor dynamic model and modified MRAS speed observer

The dynamic model equations are easier to implement and describe the characteristics of the induction motors. In order to design the estimation algorithm, the dynamic state space model of the induction motor is used with stator current and rotor flux as the state variables. 's' signifies the stationary reference frame, which in this case is applicable to the motor and the observer models. 'p' is the differential operator.

$$p \begin{bmatrix} i_s^s \\ \psi_r^s \end{bmatrix} = \begin{bmatrix} A_{11} & A_{12} \\ A_{21} & A_{22} \end{bmatrix} \begin{bmatrix} i_s^s \\ \psi_r^s \end{bmatrix} + \begin{bmatrix} B_{11} \\ 0 \end{bmatrix} v_s^s, \tag{3}$$

$$\dot{x}^s = Ax^s + Bv_s^s, \tag{4}$$

$$i_s^s = Cx^s, \tag{5}$$

where:

$$x^s = [i_s^s \psi_r^s]^T, i_s^s = [i_{ds}^s i_{qs}^s]^T, \psi_r^s = [\psi_{dr}^s \psi_{qr}^s]^T. \tag{6}$$

The electromechanical torque is given by:

$$T_e = \frac{3}{2}\frac{P}{2}\frac{L_m}{L_r}(i_{qs}^s \psi_{dr}^s - i_{ds}^s \psi_{qr}^s), \tag{7}$$

where P is the number of poles of the motor.

The above motor model used in the observer structure is given in detail in Section 3.1. The extended full-order state observer was based on adaptive control theory. The adaptive scheme is derived by making use of the stability criteria proposed by either Lyapunov or Popov. In this paper, the adaptive observer, apart from estimating the rotor flux and stator current, also makes use of a reduced-order gain matrix for stability and correction. Hence, it as an adaptive pseudoreduced order (APRO) state observer. The configuration of the extended Luenberger-based APRO speed observer with disturbance torque compensation is as shown in Figure 3, where 'A' indicates the system matrix, '^' stands for estimated values, 'X' comprises the state variables (the direct and quadrature axes stator currents and rotor fluxes), 'G' is the reduced-order observer gain matrix (chosen such that the eigenvalues of the observer are proportional to the eigenvalues of the machine to ensure stability under normal operating conditions), 'J' indicates the moment of inertia, 'p' is the differential operator, 'B_V' is the viscous friction coefficient, 'T_e^*' is the reference model electromagnetic torque, and '$\hat{T}_{dis}$' is the estimated disturbance torque. The structure of the above observer scheme with disturbance torque estimation and compensation is given below [21].

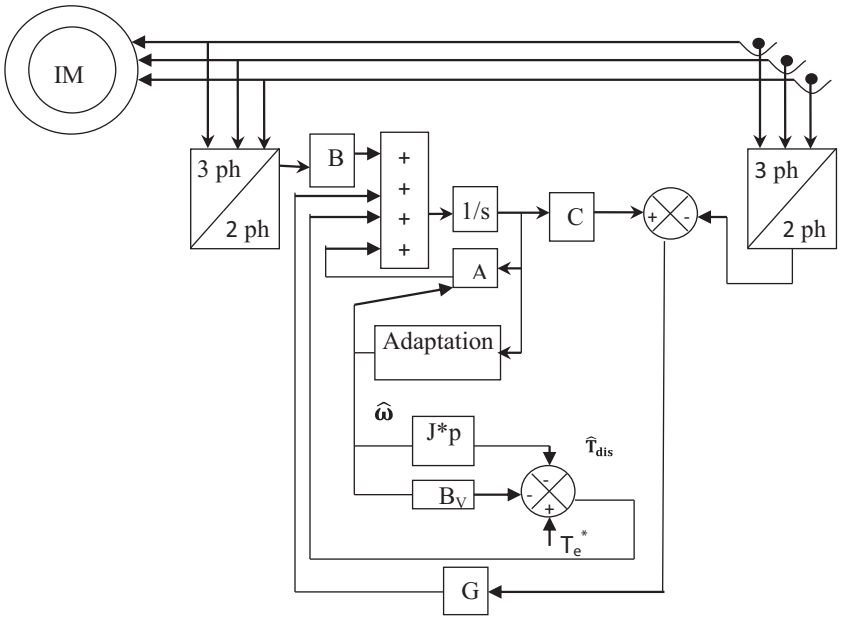

Figure 3. Extended speed observer scheme with disturbance torque compensation.

3.1. Motor model (reference model)

The following equations characterize the motor model:

$$\frac{dx}{dt} = [A]\,x + [B]\,u, \tag{8}$$

$$y = [C]\,x, \tag{9}$$

where:

$$x = [\,i_{ds}^s, i_{qs}^s, \psi_{dr}^s, \psi_{qr}^s]^T, \quad A = \begin{bmatrix} A_{11} & A_{12} \\ A_{21} & A_{22} \end{bmatrix},$$

$$I = \begin{bmatrix} 1 & 0 \\ 0 & 1 \end{bmatrix}, \quad J = \begin{bmatrix} 0 & -1 \\ 1 & 0 \end{bmatrix},$$

$$A_{11} = -\left[\frac{R_s}{\sigma L_s} + \frac{1-\sigma}{\sigma T_r}\right] I = a_{r11} I,$$

$$A_{12} = \frac{L_m}{\sigma L_s L_r}\left[\frac{1}{T_r} I - \omega_r J\right] = a_{r12} I + a_{i12} J,$$

$$A_{21} = \frac{L_m}{T_r} I = a_{r21} I,$$

$$A_{22} = \frac{-1}{T_r} I + \omega_r J = a_{r22} I + a_{i22} J,$$

$$B = \left[\frac{1}{\sigma L_s} I 0\right]^T,$$

$$C = [I, 0], \quad u = [v_{ds}^s \; v_{qs}^s]^T.$$

3.2. Disturbance torque estimation

The difference between the reference model electromagnetic torque and the estimated electromagnetic torque can be regarded as the torque disturbance. Therefore, the disturbance torque is estimated by the following equation, which makes use of the mechanical model:

$$\hat{T}_{dis} = T_e^* - J\frac{d\hat{\omega}}{dt} - B_V \hat{\omega}, \tag{10}$$

where $\hat{\omega}$ is the estimated speed.

The estimated disturbance torque is physically modeled in the observer state dynamic equation as shown:

$$\frac{d\hat{x}}{dt} = \left[\hat{A}\right]\hat{x} + [B]\,u + [G]\left(\hat{i}_s - i_s\right) + \hat{d}, \tag{11}$$

where: $\hat{d} = k\hat{T}_{dis}$,

$$\hat{y} = [C]\hat{x}, \tag{12}$$

where 'k' is an arbitrary positive gain, $\hat{i}_s$ = estimated value of stator current, and i_s = measured value of stator current.

$$\hat{A} = \begin{bmatrix} A_{11} & \hat{A}_{12} \\ A_{21} & \hat{A}_{22} \end{bmatrix}$$

$$\hat{A}_{12} = \frac{L_m}{\sigma L_s L_r}\left[\frac{1}{T_r} I - \hat{\omega}_r J\right] = a_{r12} I + \hat{a}_{i12} J$$

$$\hat{A}_{22} = \frac{-1}{T_r} I + \hat{\omega}_r J = a_{r22} I + \hat{a}_{i22} J$$

'G' is the reduced-order observer gain matrix designed for stabilizing Eq. (11). The pseudoreduced-order gain matrix is chosen as follows:

$$G = \begin{bmatrix} g_1 & g_2 \\ -g_2 & g_1 \end{bmatrix}^T. \tag{13}$$

On the basis of the pole placement technique, the observer gain matrix is determined in order to ensure the convergence of the state of the observer with that of the reference model (motor model). For faster convergence, the chosen eigenvalues are relatively more negative than the eigenvalues of the reference model. Therefore, the eigenvalues of the observer are chosen as follows:

$$g_1 = (k-1)a_{r11}, \tag{14}$$

$$g_2 = k_p k_p \geq -1, \tag{15}$$

where g_1 is dependent on the motor parameters, g_2 and k_p are arbitrarily chosen, and k is an arbitrary positive constant.

3.3. Adaptive mechanism

The adaptive scheme makes use of the Lyapunov stability criterion and the following Lyapunov candidate is defined as:

$$V = e^T e + \frac{(\hat{\omega}_r - \omega_r)^2}{\lambda}, \tag{16}$$

where λ is a positive constant.

The time derivative of V is as shown:

$$\frac{dv}{dt} = e^T \left[(A+GC)^T + (A+GC) \right] e - \frac{2\Delta\omega_r \left(e_{ids}\hat{\varphi}^s_{qr} - e_{iqs}\hat{\varphi}^s_{dr} \right)}{c} + \frac{2\Delta\omega_r}{\lambda}\frac{d\hat{\omega}_r}{dt}, \tag{17}$$

where $e_{ids} = i^s_{ds} \hat{i}^s_{ds}$ and $e_{iqs} = i^s_{qs} - \hat{i}^s_{qs}$.

The adaptation mechanism for the rotor speed is obtained by equalizing the second term with the third term:

$$\frac{d\hat{\omega}_r}{dt} = \frac{\lambda}{c}(e_{ids}\hat{\varphi}^s_{qr} - e_{iqs}\hat{\varphi}^s_{dr}). \tag{18}$$

Here, c is an arbitrary positive constant.

4. RT-Lab-based real-time simulation platform

Although several simulation tools have been employed for the design and implementation of electrical systems, they have evolved with time as technology progresses. As a result, high-performance simulation tools are now more accessible to researchers at affordable costs. The concept of real-time simulations has taken over other offline simulation methods, primarily owing to their reduced design, prototype, and test time. The mathematical solvers used in real-time systems provide accurate results without any approximation. Any real-time technology is a time-critical technology where the computer model runs at the same rate as its actual physical counterpart [22,23]. The solving technique moves forward in steps of equal duration, known as fixed step simulation. For a real-time simulator, the system states and equations have to be represented precisely and the length of the time to produce results should correspond to the time its actual physical model would take. The principle

behind this time-critical technology is illustrated in Figure 4, where the functions of variables and internal states of the model are solved at a given time step of 2 mu s. However, if the simulator is not able to solve all the operation and model calculations within the required time step, it gives rise to a phenomenon known as overrun. Therefore, in any real-time simulation platform, there is a need to avoid overruns. There are several real-time simulation tools available for consideration, like eFPGAsim, Xpc Target, and RT-Lab. The RT-Lab-based real-time simulation platform, by means of its various real-time digital simulators like ePOWERgrid, eDRIVEsim, and eFPGAsim, has a provision through which the models can be designed for a wide variety of applications including motor control.

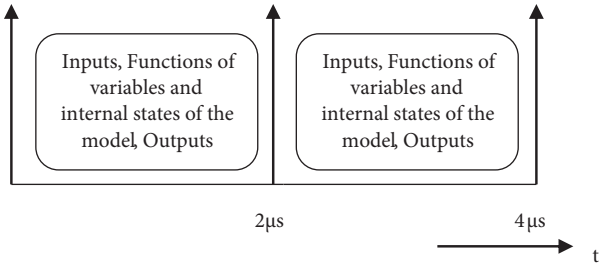

Figure 4. Fixed time step of real-time systems.

This paper makes use of RT-Lab, a technology developed by Opal-RT, as it is flexible and fully integrable with MATLAB/Simulink. The Simulink model of the observer, along with the motor, is present in the host computer/workstation and integrated with RT-Lab block sets. The workstation is connected to the OP4500 simulation target by means of TCP/IP. The OP4500 simulation target performs the processing of inputs, model calculations, and outputs in real time. The real-time platform is shown in Figure 5.

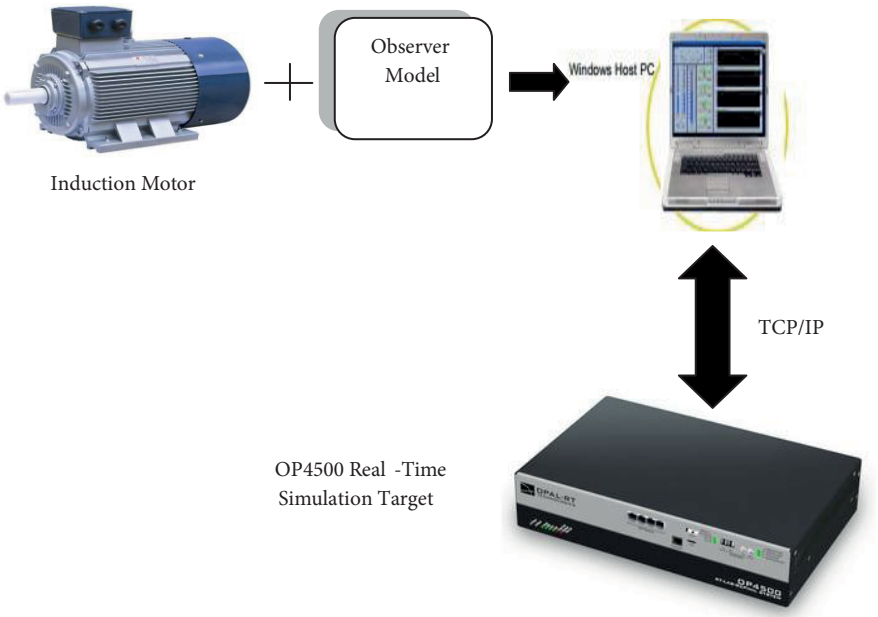

Figure 5. Distributed real-time simulation platform.

5. Offline and real-time simulation results

The drive system comprising the observer and the motor model is built in the Simulink environment of the host computer and simulated offline. The offline simulation configuration makes use of a variable step solver. In the case of real-time simulation, the system is integrated with RT-Lab block sets and makes use of a discrete time fixed step solver with a fundamental step size of 2 mu s. The OP4500 simulator developed by Opal-RT performs simulations in real time and the results can be viewed in the host computer, which acts as the front end. The model is subjected to variations in load torque and inertia coefficient in the mechanical model as shown:

1. For constant load torque of 100 Nm.
2. For a step load perturbation. (Initially at no load; after a fixed time interval, stepped up to a rated load of 150 Nm.)
3. For a step load perturbation and 25% inertia.
4. For a step load perturbation and 200% inertia.
5. For a step load perturbation and 400% inertia.

6. Discussion

The offline and real-time simulated results are observed. In all the cases, the estimated rotor speed and the estimated disturbance torque track the actual rotor speed and load torque, respectively. Alternatively, enlarged versions of rotor speed and disturbance torque waveforms are presented during steady state and transient changes to provide more clarity and distinctness in the offline and real-time results. In Figures 6a and 6b, it is observed that, at the instance of transition from no-load to rated load, the estimated speed tracks the actual speed both offline and in real time, and the disturbance torque also tracks the profile of the load torque, as shown in Figures 7a and 7b. On comparing the zoomed versions, it can be observed that the offline result of disturbance torque in Figure 7c has more distortions and is of constant magnitude, whereas the real-time result of Figure 7d is relatively smoother and the magnitude gradually decreases with time. This may be because of the difference in the solvers used offline and in real time. For constant load perturbation, compared to the offline result of Figure 8a, Figure 8b shows a smoother speed tracking in real time. The same applies to the offline torque performance of Figure 9a; Figure 9b shows the real-time tracking. As the inertia coefficient in the mechanical model is decreased (25% J), though it does not have any effect on the speed tracking performance observed in Figures 10a and 10b, closer analysis shows, as compared to the offline result in Figure 10c, that a smoother waveform with fewer distortions is obtained in real time, as shown in Figure 10d. There is a decrease in the magnitude of the oscillations in the disturbance torque at the time of transition from no-load to rated load, as shown in Figures 11a and 11b. This can be attributed to a sudden decrease in the value of the stator current error, although it stabilizes within 0.3 s. In case of increase in the inertia coefficient to double its nominal value (200% J) (although, again, the speed performance is unchanged, as shown in Figures 12a and 12b), the zoomed versions during speed transition show a smoother speed tracking in real time as compared to offline in Figures 12c and 12d. An increase in the magnitude of the oscillations in the disturbance torque at the time of transition is observed in Figures 13a and 13b due to a sudden increase in the estimated stator current, in turn affecting the convergence of the stator current error. Once again, speed tracking is unchanged

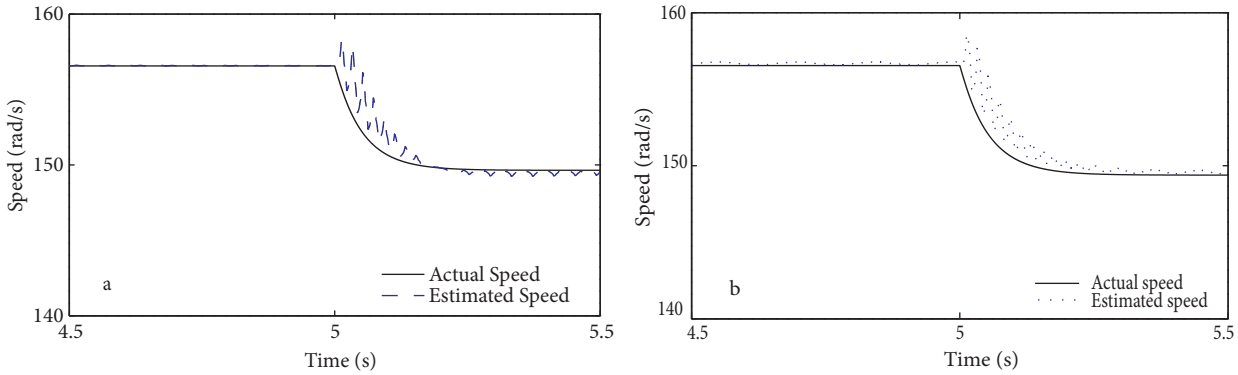

Figure 6. (a) Offline and (b) real-time estimated rotor speed.

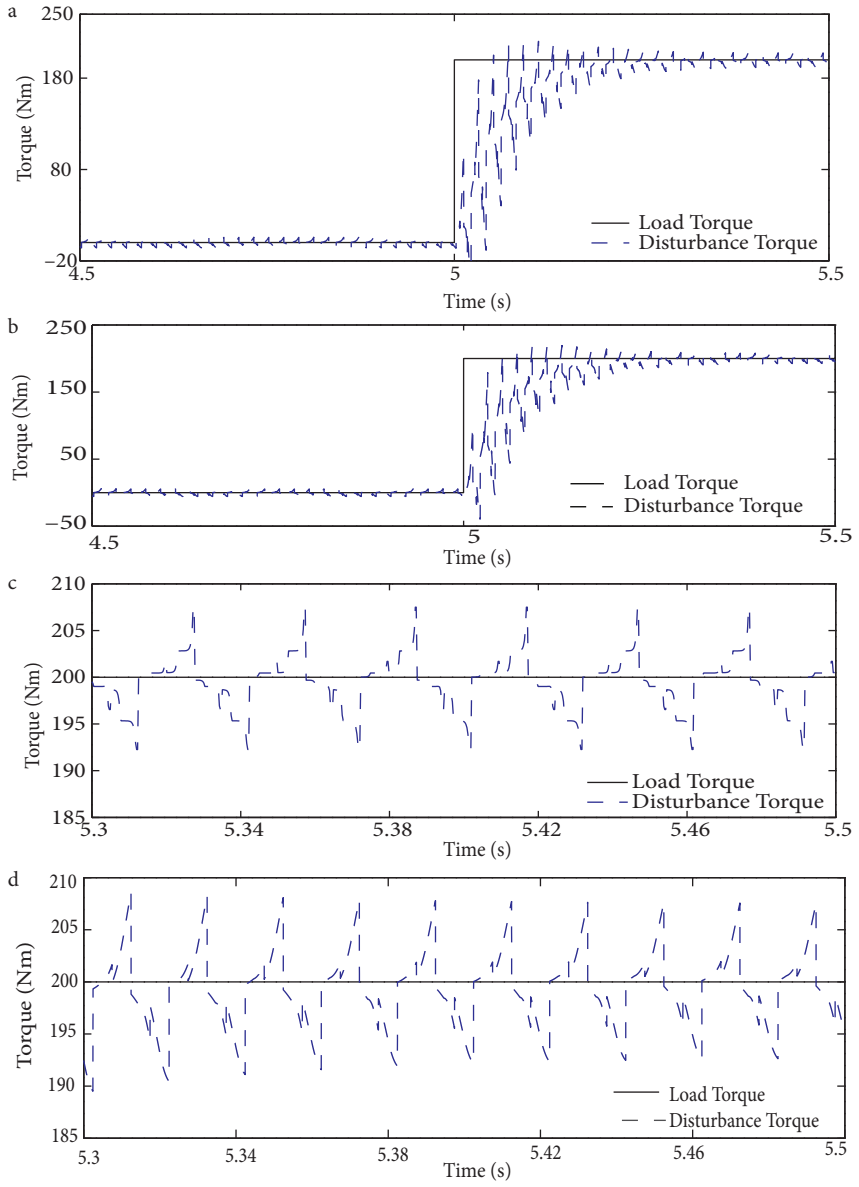

Figure 7. (a) Offline, (b) real-time estimated disturbance torque, (c) zoomed offline, and (d) zoomed real-time estimated disturbance torque.

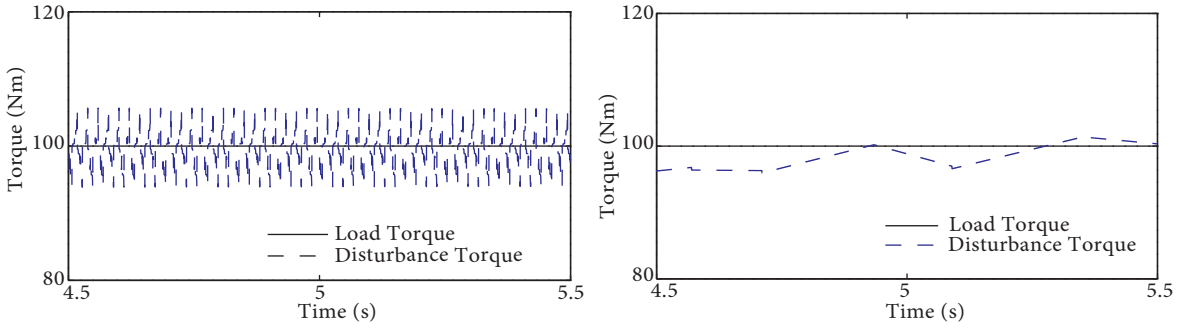

Figure 8. (a) Offline and (b) Real-time estimated rotor speed.

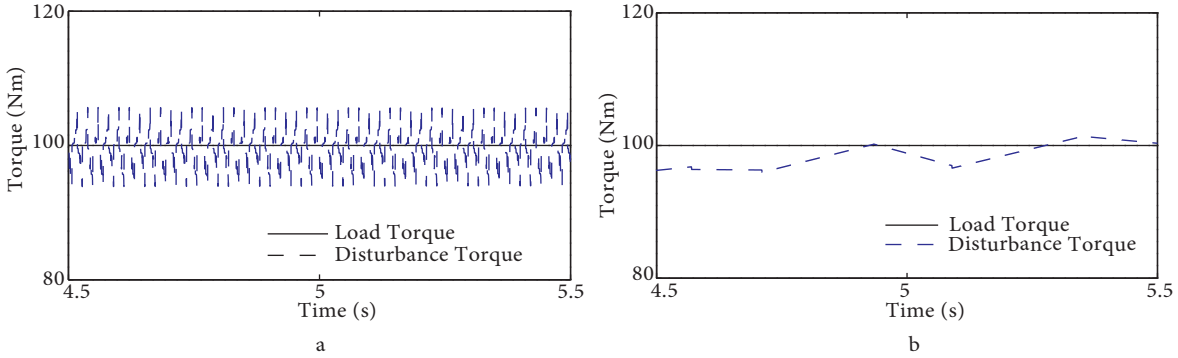

Figure 9. (a) Offline and (b) real-time estimated disturbance torque.

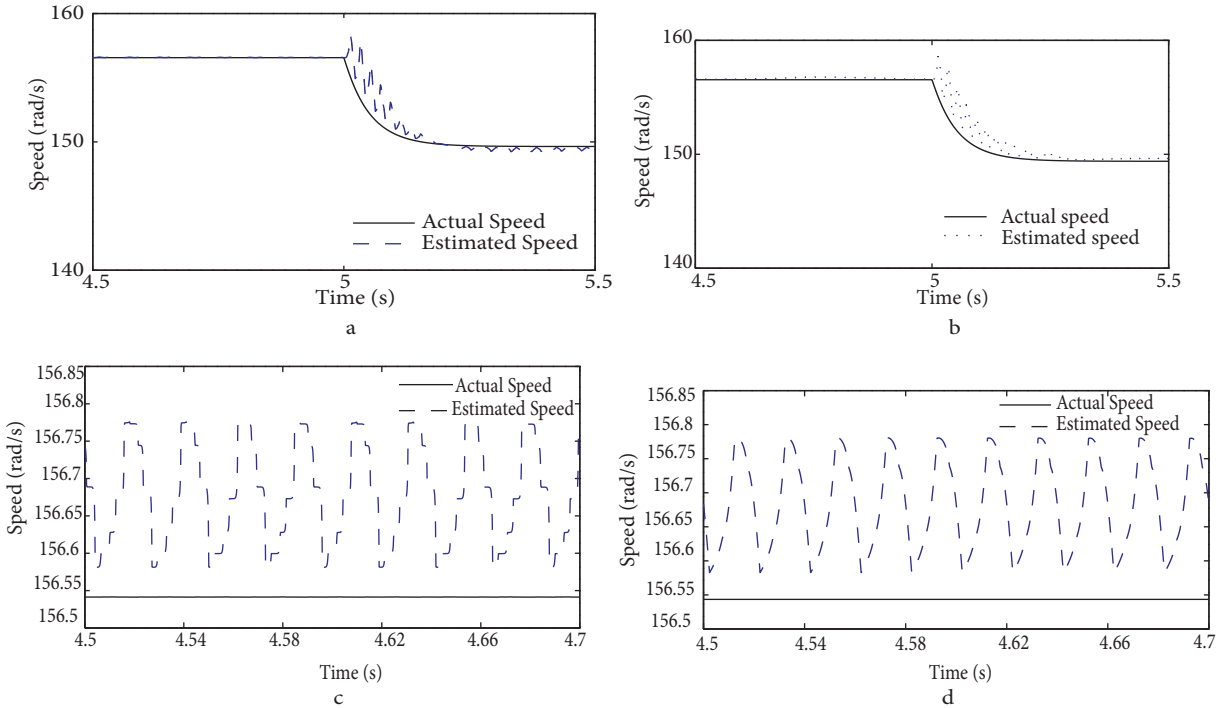

Figure 10. (a) Offline, (b) real-time estimated rotor speed, (c) zoomed offline, and (d) zoomed real-time estimated rotor speed.

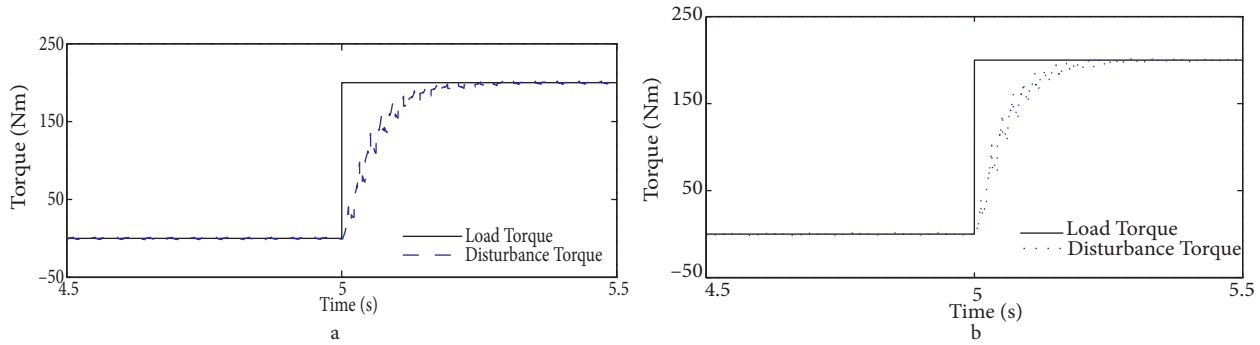

Figure 11. (a) Offline and (b) real-time estimated disturbance torque.

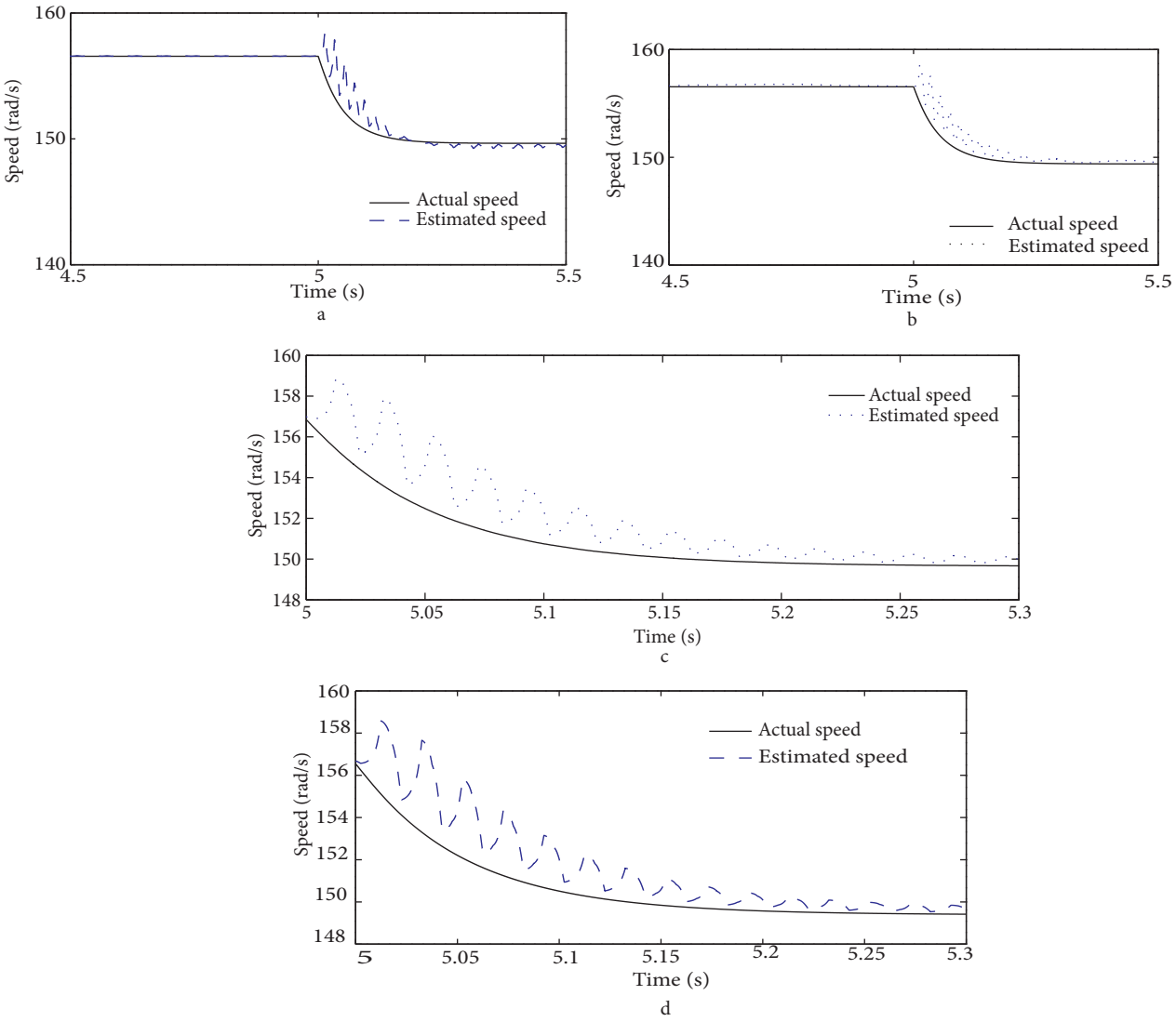

Figure 12. (a) Offline, (b) real-time estimated rotor speed, (c) zoomed offline, and (d) zoomed real-time estimated rotor speed.

even after quadrupling the inertia coefficient (400% J), as seen in Figures 14a and 14b, although again the magnitude of the torque disturbance increases and stabilizes to the rated load after 0.3 s, as shown in Figures 15a and 15b. Once again, closer scrutiny of Figure 15c shows that, although the offline result tracks the load torque well, the disturbances do not disappear completely. This is in contrast with the real-time result of Figure 15d, which shows a smoother tracking and gradual dying down of the disturbance. The purpose of observing the disturbance torque is to improve the dynamic performance of the speed observer by means of its ability to reject the effect of the load torque on the speed. Its robustness is shown through the results. The analysis is carried out in the motoring mode at speeds ranging around the base synchronous speed. The viscous friction coefficient remained constant in the mechanical model.

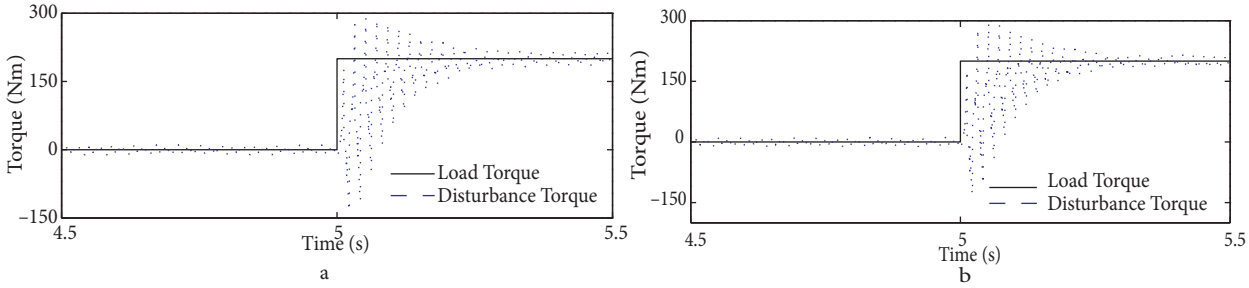

Figure 13. (a) Offline and (b) real-time estimated disturbance torque.

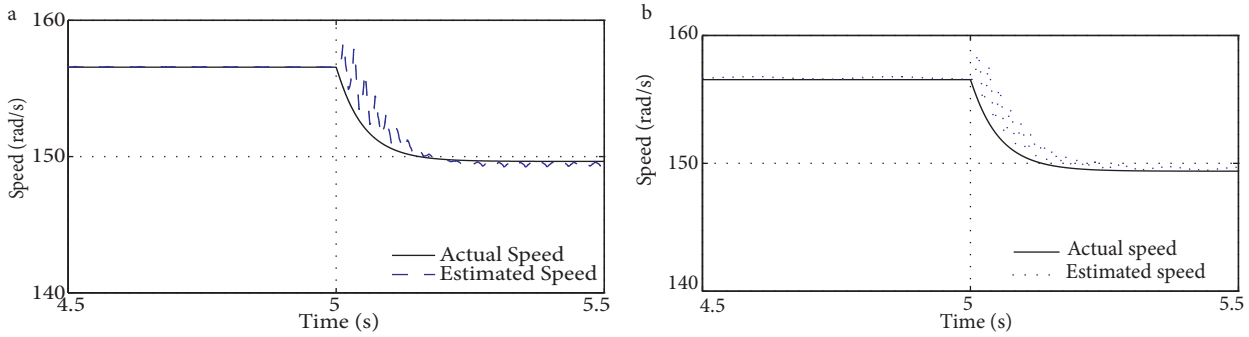

Figure 14. (a) Offline and (b) real-time estimated rotor speed.

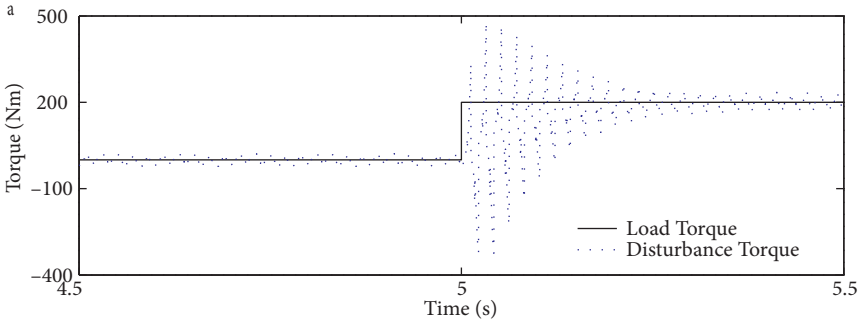

Figure 15. (a) Offline, estimated disturbance torque.

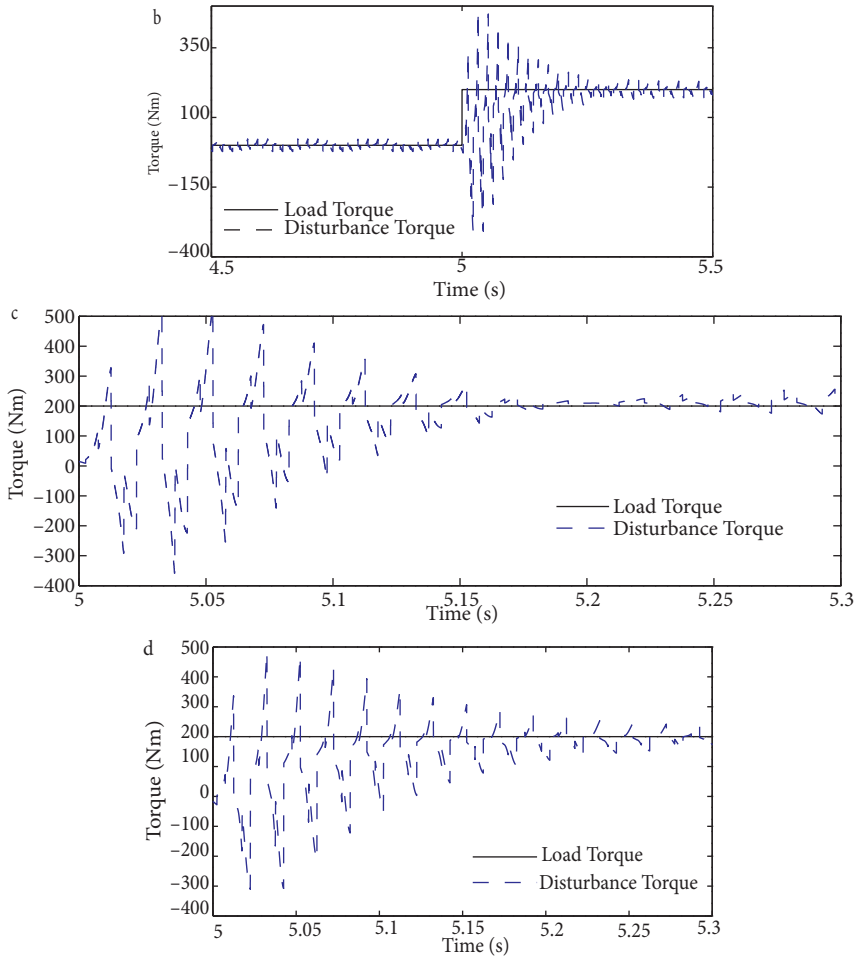

Figure 15. (b) real-time estimated disturbance torque, (c) zoomed offline, and (d) zoomed real-time estimated disturbance torque.

7. Conclusion

An extended speed observer was modeled with the estimated torque disturbance and was subjected to dynamic changes in load torque and inertia. The estimated speed and disturbance torque track the profile of the actual speed and load torque, respectively. The robustness of the improved speed and disturbance observer was proven through the offline simulation results and further validated in real time using RT-Lab. The real-time results can be considered to be the performance of the actual, physical model in wall-clock time. It can also be inferred that the real-time results are more distinct and smooth on account of the fixed step mathematical solvers used in them. Therefore, the scope can be further extended by having the physical motor (plant) externally and the observer model in the host computer and tested for hardware-in-the-loop simulation. Alternatively, in a closed loop, the controller interaction with the motor and the observer models can be tested in real time.

Nomenclature

i^s_{ds}, i^s_{qs}, i^r_{dr}, i^r_{qr}	d- and q-axis stator and rotor currents in the stationary reference frame
v^s_{ds}, v^s_{qs}	d- and q-axis stator voltages in the stationary reference frame
T_r	Rotor time constant

R_s , R_r	Stator and rotor resistance
σ	Leakage reactance
L_r , L_m , L_s	Rotor, magnetizing, and stator self-inductance
L_{ls} ,L_{lr}	Stator and rotor leakage inductances
ω_r,$\hat{\omega}_r$	Actual rotor and estimated speed
ψ^s_{ds} , ψ^s_{qs} , ψ^s_{dr} , ψ^s_{qr}	d- and q-axis stator and rotor flux linkages in the stationary reference frame
$\hat{\varphi}_d$,$\hat{\varphi}_q$	d- and q-axis estimated rotor flux linkages

References

[1] Salmasi FR, Najafabadi TR. An adaptive observer with online rotor and stator resistance estimation for induction motors with one phase current sensor. IEEE T Energy Conver 2011; 26: 959-966.

[2] Alexandru T, Gildas B. Observer scheme for state and parameter estimation in asynchronous motors with application to speed control. Eur J Control 2006; 12: 400-412.

[3] Anitha P, Chowdhury BH. Sensorless control of inverter-fed induction motor drives. Electr Pow Syst Res 2007; 77: 619-629.

[4] Yongchang Z, Zhengming Z. Speed sensorless control for three-level inverter-fed induction motors using an extended Luenberger observer. In: IEEE Vehicle Power and Propulsion Conference; 3–5 September 2008; Harbin, China. New York, NY, USA: IEEE. pp. 1-5.

[5] Holtz J. Sensorless control of induction machines – with or without signal injection. IEEE T Ind Electron 2006; 53: 7-30.

[6] Suwankawin S, Sangwongwanich S. Design strategy of an adaptive full-order observer for speed-sensorless induction-motor drives—tracking performance and stabilization. IEEE T Ind Electron 2006; 53: 96-119.

[7] Schauder C. Adaptive speed identification for vector control of induction motors without rotational transducers. IEEE T Ind Appl 1992; 28: 1054-1061.

[8] Kubota H, Matsuse K, Nakano T. DSP-based speed adaptive flux observer of induction motor. IEEE T Ind Appl 1993; 29: 160-166.

[9] Maes J, Melkebeek J. Speed sensorless direct torque control of induction motors using an adaptive flux observer. IEEE T Ind Appl 2000; 36: 778-785.

[10] Farshbaf RA, Azizian MH, Amiri K, Khosrowjerdi MJ. A comparative study of speed observers between adaptive and sliding mode approaches. In: IEEE 5th Power Electronics, Drive Systems and Technologies Conference; 5–6 February 2014; Tehran, Iran. New York, NY, USA: IEEE. pp. 556-561.

[11] Lascu C, Boldea I, Blaabjerg F. Comparative study of adaptive and inherently sensorless observers for variable speed induction motor drives. IEEE T Ind Electron 2006; 53: 57-65.

[12] Illas C, Bettini A, Griva G, Profumo F. Comparison of different schemes without shaft sensors for field oriented control drives. In: IEEE Annual Meeting IECON; 5–9 September 1994; Bologna, Italy. New York, NY, USA: IEEE. pp. 1579-1588.

[13] Gadoue SM, Giaouris D, Finch JW. Performance evaluation of a sensorless induction motor drive at very low and zero speed using a MRAS speed observer. In: IEEE International Conference on Industrial and Information Systems; 8–10 December 2008; Kharagpur, India. New York, NY, USA: IEEE. pp. 1-6.

[14] Vasic V, Vukosavic S. Robust MRAS based algorithm for stator resistance and rotor speed identification. IEEE Power Eng Rev 2001; 21: 39-41.

[15] Albu M, Horga V, Răţoi M. Disturbance torque observers for the induction motor drives. Journal of Electrical Engineering 2006; 6: 1-6.

[16] Tarek B, Abdelhafid O. Improved adaptive flux observer of an induction motor with stator resistance adaptation. Prz Elektrotechniczn 2011; 87: 325-329.

[17] Kubota H, Matsuse K. Robust field oriented induction motor drives based on disturbance torque estimation without rotational transducers. In: IEEE Industry Applications Society Annual Meeting; 4–9 October 1992. New York, NY, USA: IEEE. pp. 558-562.

[18] Krzeminski Z. Observer of induction motor speed based on exact disturbance model. In: IEEE 13th International Power Electronics and Motion Control Conference; 1–3 September 2008; New York, NY, USA: IEEE. pp. 2294-2299.

[19] Krzeminski Z. A new speed observer for control system of induction motor. In: IEEE International Conference on Power Electronics and Drive Systems; 27–29 July 1999; Hong Kong. New York, NY, USA: IEEE. pp. 555-560.

[20] Landau YD. Adaptive Control - The Model Reference Approach. 1st ed. New York, NY, USA: Taylor & Francis, 1979.

[21] Zhiwu H, Yongteng S, Weihua G, Xiaohong N. Stability analysis and design of adaptive observer based on speed sensorless induction motor. In: IEEE Proceedings of the 26th Chinese Control Conference; 26–31 July 2007; Zhangjiajie, China. New York, NY, USA: IEEE. pp. 28-32.

[22] Mikkili S, Prattipati J, Panda AK. Review of real-time simulator and the steps involved for implementation of a model from MATLAB/Simulink to real-time. J Inst Eng India B 2014; 96: 179-196.

[23] Kaddouri A, Khodabakhchian B, Dessaint LA, Champagne R, Snider L. A new generation of simulation tools for electric drives and power electronics. In: IEEE International Conference on Power Electronics and Drive Systems; 27–29 July 1999; Hong Kong. New York, NY, USA: IEEE. pp. 348-354.

Appendix. The motor ratings and the parameters considered for simulation are given as follows: a 1 HP, three-phase, 415 V, 50 Hz, star-connected, four-pole induction motor with equivalent parameters: $R_S = 0.087$ Ω, $R_r = 0.228$ Ω, $L_{ls} = L_{lr} = 0.8$ mH, $L_m = 34.7$ mH, inertia, $J = 1.662$ kg m^2, friction factor = 0.1.